# Full-Scale Accelerated Pavement Testing of Geogrid Stabilized Roads

J.S. Tingle, G.J. Norwood & W.J. Robinson
*US Army Engineer Research and Development Center, USA*

M.H. Wayne
*Tensar International, Inc., USA*

Jayhyun Kwon
*Kennesaw State University, USA*

ABSTRACT: The use of geogrid products to stabilize flexible pavement systems has been well documented, particularly for paved and unpaved roads over soft subgrades. However, the quantification of the benefit of incorporating the geogrids requires further investigation. The objective of this study was to compare the performance of different flexible pavement sections with and without geogrid reinforcement to attempt to quantify the potential benefit of the geogrid inclusion in terms of extended service life and reduced pavement structure. To achieve this objective, full-scale test sections were constructed including unstabilized and stabilized test items with different pavement structures. Standard construction equipment and methods were used to build the model pavement section and replicate field conditions. Each individual test item was trafficked with a Heavy Vehicle Simulator (HVS) equipped with a dual-wheel tandem axle gear loaded to 20,000 lbs and a tire pressure of 120 psi. This paper describes the testing and the analysis of the rutting performance of the different test items. The results demonstrate that the inclusion of the geogrid products provides enhanced rutting resistance compared to unstabilized sections. In addition, the performance comparison also demonstrates that the inclusion of geogrid reinforcement within the base course can allow a reduction in the base course thickness, and/or in some cases, the asphalt concrete surface thickness.

## 1 INTRODUCTION

### 1.1 *Background*

As material costs rise and agency budgets decline, transportation officials are exploring nontraditional pavement design and construction materials and methods to maintain and improve their deteriorating transportation networks. The use of geosynthetics in pavement structures has been growing exponentially, even to the point that some applications are becoming the norm rather than the exception. These products have been shown to be effective in improving pavement performance, reducing overall pavement thickness, and in reducing construction costs. Research efforts have been performed to determine the performance benefit of some biaxial and multi-axial geogrids [Kim et al. (2005); Aran, S. (2006); Christopher et al. (2001); Barksdale et al. (1989); Haas et al. (1988); Al Qadi et al. (1988); Perkins and Ismeik (1999); Tingle and Jersey (2007); Berg et al. (2000); Norwood and Tingle (2014)]. As new geosynthetic products are developed, full-scale performance data are needed to provide quantifiable benefits to pavement designers.

### 1.2 *Objective*

The objective of this paper is to assemble the results from multiple pavement test sections subjected to accelerated traffic to assess the rutting performance of pavements stabilized with multi-axial geogrids. Full-scale flexible pavement sections were constructed and trafficked to provide performance data for comparing the effectiveness of pavement sections stabilized with multi-axial geogrids to unstabilized flexible pavement sections. The summarized data includes multiple flexible pavement surface types/thicknesses, two base thicknesses, and two subgrade strength conditions. The compilation of test results presented in this paper offers an opportunity to assess performance for a wider variety of test conditions than the assessment of singular pavement sections alone.

## 2 PERFORMANCE DATA COLLECTION

### 2.1 *Description of Pavement Test Sections*

Figure 1 shows a combined profile view of nine different full-scale pavement test sections constructed and trafficked at the U.S. Army Engineer Re-

search and Development Center (ERDC). Each test section consisted of a 8-ft-wide by 50-ft-long testing area. The subgrade for the test sections consisted of nominal 28-36 in. of high-plasticity clay (CH) placed to achieve a target California Bearing Ratio (CBR) value of either 3% or 6%. The aggregate base course consisted of 6-8 in. of a crushed limestone. Sections A, C, F, and G were stabilized by placing a multi-axial geogrid at the base-subgrade interface. The test section surfacing for Sections A and B consisted of a double bituminous surface treatment (DBST), and the surfacing for Sections C-H consisted of 2-4 in. of dense-graded hot mix asphalt (HMA). All construction and traffic testing occurred under ERDC's Hangar 2 pavement testing facility, which minimized the potential for moisture variations due to environmental factors. The test sections contained a suite of instrumentation consisting of asphalt strain gauges, earth pressure cells, moisture probes, pore water pressure transducers, and temperature probes. Detailed information on the instrumentation is being published in an ERDC Technical Report (Robinson et al. 2017). However, a detailed description and discussion of the instrumentation response is beyond the scope of this paper.

The test sections were trafficked with ERDC's Heavy Vehicle Simulator (HVS) simulating typical highway loadings. The configuration used for testing consisted of a tandem-axle dual wheel gear loaded to a nominal load of 20,000 lb. Tire pressures were maintained at 120 psi throughout testing.
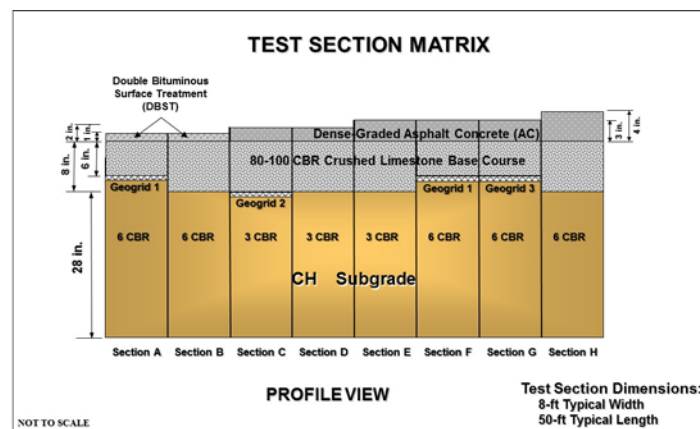


Figure 1. Profile view of matrix of pavement test sections included in this study.

## 2.2 Material Description

A local high-plasticity clay was used to construct the 28- to 36-in.-thick test section subgrade. A particle size analysis indicated that the material consisted of 96.8% fines passing the No. 200 sieve. The clay had a liquid limit (LL) of 65%, a plastic limit (PL) of 27%, and a plasticity index (PI) of 38%, as determined by ASTM D4318 (2010). According to the Unified Soil Classification System (2011), the soil

was classified as a high-plasticity clay (CH) and an A-7-6 according to the American Association of State and Highway Transportation Officials (AASHTO, 2012)) classification system. Modified proctor compaction tests (ASTM D1557, 2012) were performed to determine the relationship between moisture content and dry density. The maximum dry density was found to be 101.8 pcf at an optimum moisture content of 18.6%. Laboratory CBR tests (ASTM D1883, 2016) were performed to determine a target moisture content required to produce the targeted 3% or 6% CBR.

The geogrids evaluated in this study were all multi-axial geogrid products manufactured from a punched and drawn polypropylene sheet. The geogrids have a hexagonal structure forming a series of triangular apertures. Nominal index properties provided for each geogrid are presented in Table 1.

Table 1. Description of Geogrids 1-3

| Index Property | Geogrid 1 | | | Geogrid 2 | | | Geogrid 3 | | |
| --- | --- | --- | --- | --- | --- | --- | --- | --- | --- |
| | Long. (in.) | Diag. (in.) | Trans (in.) | Long. (in.) | Diag. (in.) | Trans (in.) | Long. (in.) | Diag. (in.) | Trans (in.) |
| Rib pitch | 1.6 | 1.6 | -- | 1.6 | 1.6 | -- | 1.3 | 1.3 | -- |
| Mid-rib depth | -- | 0.05 | 0.05 | -- | 0.05 | 0.05 | -- | 0.06 | 0.05 |
| Mid-rib width | -- | 0.04 | 0.05 | -- | 0.04 | 0.04 | -- | 0.02 | 0.03 |

Crushed limestone with a maximum aggregate size of 1.5 in. was used to construct the flexible aggregate base course. ASTM D2487 was used to determine that the base course was comprised of 71.5% gravel, 23.3% sand, and 5.2% non-plastic fines passing the No. 200 sieve. The coefficient of curvature (Cc) was calculated as 2.71, and the coefficient of uniformity (Cu) was 21.16. The crushed limestone aggregate base was classified as a well-graded gravel with silt and sand (GW-GM) according to the USCS and an A-1-a according to the AASHTO procedure. Modified proctor compaction tests were performed in accordance with ASTM D1557 Method C Modified to determine a maximum dry density of 146.7 pcf at an optimum moisture content of 5.9%.

Sections A and B were surfaced with a double bituminous surface treatment (DBST) typical of that used for low-volume roads. A CRS-2P asphalt emulsion was used as the binder at application rates of 0.3 gsy and 0.4 gsy for the initial and final layers, respectively. A uniform graded crushed limestone aggregate with a maximum aggregate size of 0.75 in. and 5% passing the No. 4 sieve was placed at a rate of 28 lb/yd$^2$.

The wearing surface for Sections C-H was comprised of a 3/8-in. nominal maximum aggregate size (NMAS) dense-graded HMA surface mixture. The asphalt mixture was one that is representative of local highway mixtures used on medium-traffic level roadways in Mississippi. The dense-graded HMA

used a PG 67-22 binder with an asphalt content of 5.0-5.5% for different sections. The HMA was comprised of 43-46% gravel, 38-42% sand, and 4-5% non-plastic fines passing the No. 200 sieve. The VMA ranged from 15.1-15.4%.

## 2.3 Test Section Construction Data

Detailed as-built construction data for each test section are provided elsewhere [Jersey et al. (2012); Norwood and Tingle, 2014; Norwood and Tingle, 2014]. However, Table 2 provides a brief summary of the key test section construction data. The data indicate that the CH subgrade was constructed to a relatively uniform dry density for each subgrade strength, ranging from 83.0 to 83.6 pcf for the 3% CBR subgrade sections (C-E) and 88.0-88.9 pcf for the 6% CBR subgrade sections (A, B, F, G, & H). As shown, the actual subgrade strengths were similar to the target values. The crushed limestone dry densities ranged from 134.5-150.1 pcf, showing slightly more variability between sections, while the CBR strengths ranged from 90.5-100+% for all sections. Additionally, the thicknesses for all sections were reasonably close to target values with the exception of Section B which had a 6.2-in.-thick base instead of the target 8.0 in.

Table 2. Detailed Construction Data

| Property | Section A | Section B | Section C | Section D | Section E | Section F | Section G | Section H |
|---|---|---|---|---|---|---|---|---|
| CH Subgrade Properties | | | | | | | | |
| Wet Density (pcf) | 115.5 | 116.4 | 113.8 | 114.0 | 112.9 | 116.5 | 116.6 | 116.9 |
| Dry Density (pcf) | 88.0 | 88.8 | 83.6 | 83.5 | 83.0 | 88.5 | 88.7 | 88.9 |
| Nuclear Moisture Content (%) | 31.3 | 31.1 | 36.1 | 36.1 | 36.2 | 31.6 | 31.6 | 30.0 |
| Oven-Dried Moisture (%) | 35.3 | 33.1 | 37.0 | 37.9 | 38.9 | 32.7 | 32.6 | 34.1 |
| In-Place CBR (%) | 6.0 | 6.2 | 3.1 | 2.9 | 2.8 | 5.9 | 5.9 | 5.9 |
| Crushed Limestone Properties | | | | | | | | |
| Wet Density (pcf) | 140.5 | 140.3 | 153.2 | 153.8 | 154.6 | 138.8 | 141.5 | 143.0 |
| Dry Density (pcf) | 135.6 | 135.6 | 148.8 | 149.7 | 150.1 | 134.5 | 137.2 | 138.1 |
| Nuclear Moisture Content (%) | 3.6 | 3.5 | 2.9 | 2.7 | 3.0 | 3.3 | 3.3 | 3.6 |
| Oven-Dried Moisture (%) | 2.2 | 2.5 | 2.3 | 2.1 | 1.4 | 3.0 | 3.2 | 2.4 |
| In-Place CBR (%) | 100 | 100 | 90.5 | 100 | 100 | 98.6 | 100 | 95.3 |
| Thickness (in.) | 6.2 | 7.7 | 7.4 | 8.1 | 7.9 | 5.8 | 5.9 | 7.7 |
| Hot-Mix Asphalt Properties | | | | | | | | |
| Thickness (in.) | 1.0 | 1.0 | 2.0 | 2.0 | 3.0 | 3.2 | 3.2 | 4.0 |

## 2.4 Traffic Testing of Sections

Traffic testing on the test sections was performed utilizing a dual-wheel tandem axle gear configuration (Figure 2) on the ERDC HVS. The axle configuration was subjected to a 20,000-lb nominal load and was verified prior to testing by weighing each axle with portable aircraft wheel scales. Tire pressures were monitored and maintained at 120 psi throughout traffic testing. The equivalent single axle load factor for this configuration is 2.08; therefore, each pass of the HVS was equal to 2.08 equivalent single axle loads (ESALS). Each test section was trafficked utilizing a normally distributed bi-directional traffic pattern with a total lateral wander width of 3 feet. The environmental chamber was maintained at a target pavement temperature of 77°F, with an allowable range of ±10°F during trafficking, to minimize the effect of temperature variation on rutting performance.



Figure 2. Dual-wheel tandem axle gear used to traffic the test sections.

## 3 RESULTS

### 3.1 Rutting and Permanent Surface Deformation

The predominant distress and failure mechanism for all pavement sections was rutting. Forensics showed that none of the geogrids ruptured at the completion of traffic. Rut depth measurements were collected at predetermined traffic levels throughout the testing period. Rut depth measurements were made by placing a metal straight edge across the traffic lane at designated cross-sections and measuring the maximum rut depth to 1/16" using a machined depth wedge. The maximum rut depth includes permanent surface deformation and upheaval along the edge of the traffic pattern.

Figure 3 presents a comparison of the rutting performance of the unstabilized pavement test sections excluding Section B that was surfaced with a DBST. The figure shows that the rutting performance improves as the thickness of the asphalt concrete surface increases, noting that Section H also had a higher subgrade CBR of 6% compared to Sections D and E. Figure 3 provides confidence that the rutting performance data are following expected trends.

Figure 4 shows the rutting performance for Sections C-E that were constructed over a 3% CBR subgrade. Figure 4 shows that the rutting performance of Section C with the inclusion of Geogrid 2 was clearly better than that of the unstabilized control Section D as well as the unstabilized Section E which was surfaced with 3 in. of HMA versus the 2-in. HMA surfacing used for Sections C and D.

Figure 5 illustrates the rutting performance for Sections A, B, F, G, & H that were constructed over a 6% CBR subgrade. Figure 5 shows that the two

sections surfaced only with a 1-in. DBST (Sections A & B) rutted the fastest as expected with the stabilized Section A providing better rutting resistance than the unstabilized Section B. A comparison of Sections F-H shows that Section G provided the best rutting resistance, followed by Section F, with Section H providing the worst rutting resistance of the 3 sections constructed over a 6% CBR subgrade and surfaced with dense-graded HMA. These data indicate that both Geogrids 1 and 3 provided significant improvement to the pavement sections' rutting resistance, even greater than an unstabilized section with an additional inch of HMA and 2 in. additional crushed limestone base course. Further review indicates that Geogrid 3 performed slightly better than Geogrid 1 for these test conditions.
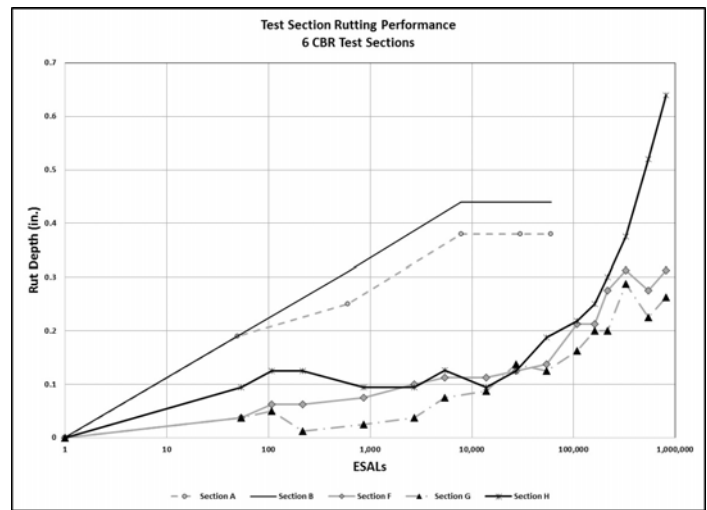


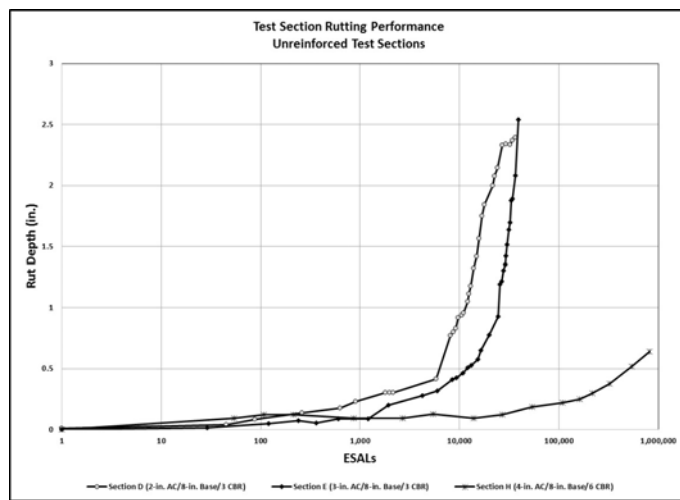Figure 5. Rutting performance of test sections with a 6% CBR subgrade.



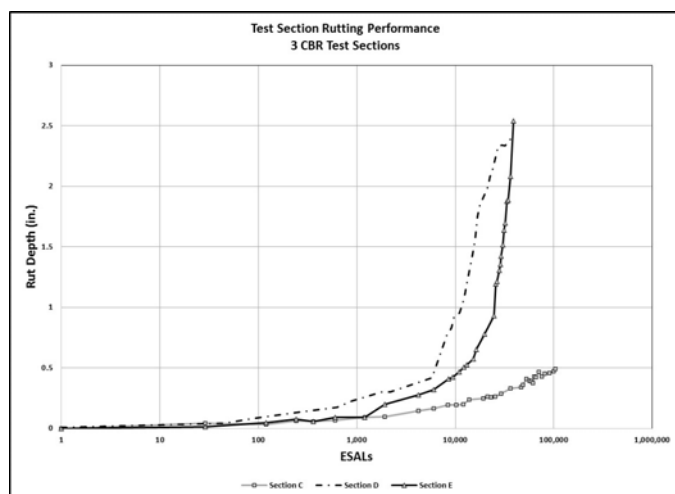Figure 3. Rutting performance of unstabilized test sections.



Figure 4. Rutting performance of test sections with a 3% CBR subgrade.

### 3.2 *Traffic Benefit Ratio*

One simplistic method of quantifying the relative benefit of a geogrid within the pavement structure is the Traffic Benefit Ratio (TBR). This quantity provides an index of the performance benefit of the geogrid relative to an unstabilized structure. It has been used to quantify and compare life-cycle costs in a cost-benefit analysis. Only the 3% CBR sections have an unstabilized pavement section (Section D) with the same layer structure as a stabilized pavement structure (Section C) to allow for computation of the TBR. The TBR values computed for the 3% CBR pavement sections described in this study are summarized in Table 3. The TBR values measured during this study were in excess of 16 for Geogrid 2 relative to the control section (D) constructed with a 2-in. thick HMA surface. In addition, TBR values were calculated for Section F which was surfaced with 3 in. of HMA to demonstrate the TBR computation resulting from adding 1 in. of HMA to the design. The data in Table 3 indicate that it was more beneficial to add Geogrid 2 to the pavement structure than to include an additional 1 in. of HMA.

It is important to note that TBR values from this study should not be applied in design as direct multipliers to unstabilized design unless the pavement structure, materials and subgrade conditions are essentially identical to those tested in this study. Further, excessive TBR values, such as those observed with Geogrid 2 should not be interpreted as evidence that the stabilized pavement will have an infinite lifespan. Many factors such as layer thicknesses, base course quality, and subgrade strength will influence the performance benefit provided by geogrid reinforcement. Therefore, results from experiments like this must be properly interpreted and properly incorporated into design methodologies to insure that the desired stabilized pavement performance re-

sults are achieved. Results of experiments such as this are most appropriate to provide a means of validating the performance predicted by design approaches that have incorporated the benefit of geogrid reinforcement.

Table 3. Traffic Benefit Ratios for 3% CBR Sections

| Test Section | Rutting Level | | | |
|---|---|---|---|---|
| | 0.25 in. | 0.50 in. | 0.75 in. | 1.0 in. |
| C | 16.6 | 16.7 | – | – |
| D | – | – | – | – |
| E | 1.9 | 2.3 | 2.4 | 2.2 |

### 3.3 *Effective Structural Capacity*

In order to quantify the structural contribution of the geogrids, an effective structural number was calculated for each test section using the AASHTO Pavement Design Guide (1993). The effective structural number was calculated from the AASHTO nomograph using the subgrade CBR strength converted to modulus, the as-built layer thicknesses, the applied ESALs, and a reliability of 90%. Once the effective structural number for the test section was computed, the AASHTO structural number equation was used to compute the effective structural coefficient of the base course layer, assuming the typical structural coefficient for the asphalt concrete of 0.44. The effective structural coefficient provides a means of comparing test sections of varying layer thicknesses. Table 4 summarizes the effective base coefficient for each test section based upon the ESALs required to produce 0.5- and 1.0-in. of rutting. The calculations indicate the different geogrid items had similar effective base layer structural coefficients, ranging from 0.27-0.29 for the HMA surfaced sections. The calculations show similar effective base layer structural coefficients ranging from 0.09-0.17 for the unstabilized sections, with 0.12-0.14 being typical. These values for the unstabilized effective base layer coefficient agree reasonably with the typical 0.14 base layer coefficient used by AASHTO. The higher effective base layer coefficients for the stabilized sections show a significant increase in the structural capacity over the unstabilized sections. It should be noted that some of the test sections did not actually reach the failure criteria of 1-in. of rutting; therefore, the structural coefficients presented should be considered conservative estimates.

Table 4. Effective Structural Capacity of Sections

| Property | Section A | Section B | Section C | Section D | Section E | Section F | Section G | Section H |
|---|---|---|---|---|---|---|---|---|
| Base Thickness (in.) | 6.2 | 7.7 | 7.4 | 8.1 | 7.9 | 5.8 | 5.9 | 7.7 |
| Asphalt Thickness (in.) | 1.0 | 1.0 | 2.0 | 2.0 | 3.0 | 3.2 | 3.2 | 4.0 |
| Unreinforced Structural Number | 1.31 | 1.52 | 1.92 | 2.01 | 2.43 | 2.22 | 2.24 | 2.84 |
| Passes to Failure (ESALs) (1-in. rutting) | -- | -- | 104,000+ | 11,500 | 24,821 | 811,200+ | 811,200+ | 811,200+ |
| Effective Structural Number | -- | -- | 2.87+ | 2.03 | 2.30 | 3.08+ | 3.08+ | 3.08+ |
| Effective Base Coefficient (1-in. rutting) | -- | -- | 0.27+ | 0.14 | 0.12 | 0.29+ | 0.28+ | 0.17+ |
| Passes to Failure (ESALs) (1/2-in. rutting) | 60,000+ | 60,000+ | 104,000 | 6,351 | 11,960 | 811,200+ | 811,200+ | 500,000 |
| Effective Structural Number | 2.04+ | 2.04+ | 2.87 | 1.84 | 2.04 | 3.08+ | 3.08+ | 2.86 |
| Effective Base Coefficient (1/2-in. rutting) | 0.26+ | 0.21+ | 0.27 | 0.12 | 0.091 | 0.29+ | 0.28+ | 0.14 |

## 4 CONCLUSIONS

This paper describes the accelerated testing and the analysis of the rutting performance of eight different pavement sections. The research results demonstrate that the inclusion of the multi-axial geogrid products provides enhanced rutting resistance compared to unstabilized sections. The rutting performance improvement was demonstrated in terms of stabilized pavement sections sustaining more ESALs than comparable unstabilized pavement sections. In addition, analyses in terms of the TBR showed very high TBR values for the stabilized pavement section compared to the unstabilized control section as well as an unstabilized control section with an additional inch of asphalt concrete surfacing. Finally, back calculation of effective structural numbers for the stabilized pavement sections showed higher effective structural numbers than those computed for the unstabilized pavement sections. Effective base layer coefficients were computed based upon the effective structural numbers, and it was observed that stabilized sections surfaced with dense-graded asphalt concrete had effective base layer coefficients ranging from 0.27-0.29, much higher than the typical 0.14. In addition, the performance comparison also demonstrates that the inclusion of multi-axial geogrid reinforcement within the base course can allow a reduction in the base course thickness, and/or in some cases, the asphalt concrete surface thickness. For example, Section A performed better than Section B, which included 2 additional inches of crushed limestone base material (8 in. vs. 6 in.). In addition, Section C performed better than Section E that included an additional inch of asphalt concrete surfacing (3 in. vs. 2 in.). Likewise, Sections F and G performed better than Section H which included two additional inches of crushed limestone base material (8 in. vs. 6 in.) and an additional inch of asphalt concrete surfacing (4 in. vs. 3 in.). Therefore, the research presented in this paper demonstrates that geogrid placed within flexible pavement structures provides extended service life and/or the potential to reduce pavement structural thickness for equivalent performance for the range of pavement conditions tested.

## 5 ACKNOWLEDGEMENTS

## 6 REFERENCES

Al-Qadi, I.L., T.L. Brandon, R.J. Valentine, B.A. Lacina, and T.E. Smith. Laboratory Evaluation of Geosynthetic-Reinforced Pavement Sections. In *Transportation Research Record 1188*, TRB, National Research Council, Washington, D.C., 1988, pp. 25-31.

American Society for Testing and Materials (ASTM). 2010. *Standard test methods for liquid limit, plastic limit, and plasticity index of soils*. Designation: D 4318-10e1. West Conshohocken, PA

American Society for Testing and Materials (ASTM). 2011. *Standard practice for classification of soils for engineering purposes (Unified Soil Classification System)*. Designation: D 2487-11. West Conshohocken, PA.

American Society for Testing and Materials (ASTM). 2012. *Standard test methods for laboratory compaction characteristics of soil using modified effort (56,000 ft-blf/ft$^3$ (2,700 kN-m/m$^3$))*. Designation: D 1557-12e1. West Conshohocken, PA.

American Society for Testing and Materials (ASTM). 2016. *Standard test method for California Bearing Ratio (CBR) of laboratory-compacted soils*. Designation: D 1883-16. West Conshohocken, PA.

American Society for Testing and Materials (ASTM). 2015. *Standard test methods for in-place density and water content of soil and soil-aggregate by nuclear methods (shallow depth)*. Designation: D 6938-15. West Conshohocken, PA.

American Society for Testing and Materials (ASTM). 2009. *Standard test method for CBR (California Bearing Ratio) of soils in place*. Designation: D 4429-09a. West Conshohocken, PA.

Aran, Shirwan. Base Reinforcement with Biaxial Geogrid. In *Transportation Research Record 1975*, TRB, National Research Council, Washington, D.C., 2006, pp. 115-123.

Association of American Highway and Transportation Officials (AASHTO). 2012. *Standard Specification for Classification of Soils and Soil-Aggregate Mixtures for Highway Construction Purposes*, AASHTO M 145, Washington, D.C.

Association of American Highway and Transportation Officials (AASHTO). 2013. *Standard Method of Test for Bulk Specific Gravity (G$_{mb}$) of Compacted Hot Mix Asphalt (HMA) Using Saturated Surface-Dry Specimens*, AASHTO T 166, Washington, D.C.

Association of American Highway and Transportation Officials (AASHTO). 1993. *AASHTO Guide for Design of Pavement Structures*, Washington, D.C.

Barksdale, R., S. Brown, and F. Chan. *NCHRP Report 315: Potential Benefits of Geosynthetics in Flexible Pavement Systems*. TRB, National Research Council, Washington, D.C., 1989.

Berg, R.R., B.R. Christopher, and S.W. Perkins. *Geosynthetic Reinforcement of the Aggregate Base/Subbase Courses of Flexible Pavement Structures*. GMA White Paper II. Geosynthetic Materials Association, Roseville, MN, 2000.

Christopher, B.R., R.R. Berg, and S.W. Perkins. *Geosynthetic Reinforcements in Roadway Sections Report*. NCHRP Project 20-7 Task 112. TRB, National Research Council, Washington, D.C., 2001.

Haas, R., J.Walls, and R.G. Carroll. Geogrid Reinforcement of Granular Bases in Flexible Pavements. In *Transportation Research Record 1188*, TRB, National Research Council, Washington, D.C., 1988, pp. 19-27.

Jersey, S.R., Tingle, J.S., Norwood, G.J., Kwon, J., and Wayne, M. Full-Scale Evaluation of Geogrid-Reinforced Thin Flexible Pavements. In *Transportation Research Record 2310*, TRB, National Research Council, Washington, D.C., 2012, pp. 61-71.

Kim, Woon-Hyung, T.B. Edil, C.H. Benson, and B.F. Tanyu. Structural Contribution of Geosynthetic-Reinforced Working Platforms in Flexible Pavement. In *Transportation Research Record 1936*, TRB, National Research Council, Washington, D.C., 2005, pp.43-50.

Norwood, Gregory J., and Jeb S. Tingle. *Performance of Geogrid-Stabilized Flexible Pavements*. No. ERDC/GSL-TR-14-28. U.S. Army Engineer Research and Develop-

ment Center, Geotechnical and Structures Laboratory, Vicksburg, MS, 2014.

Perkins, S.W., and M. Ismeik. A Synthesis and Evaluation of Geosynthetic Reinforced Base Layers in Flexible Pavements: Part I. In *Geosynthetics International*, Vol. 4, No. 6, 1999, pp. 549-605.

Robinson, J., Norwood, G.J., and Tingle, J.S. *Performance of Flexible Pavements Stabilized with Multi-Axial Geogrids.* ERDC DRAFT Report. U.S. Army Engineer Research and Development Center, Vicksburg, MS, 2017.

Tingle, J.S., and S.R. Jersey. Empirical Design Methods for Geosynthetic-Reinforced Low-Volume Roads. In *Transportation Research Record 1989*, TRB, National Research Council, Washington, D.C., 2007, pp. 91-101.